LA-UR-01- 1454

TITLE: STRUCTURAL AND RF ANALYSIS OF LANL 2 GAP, 350 MHZ SPOKE RESONATOR CAVITY

AUTHOR(S): Richard P. LaFave LANSCE-1

SUBMITTED TO: Informal Distribution / Internal and External

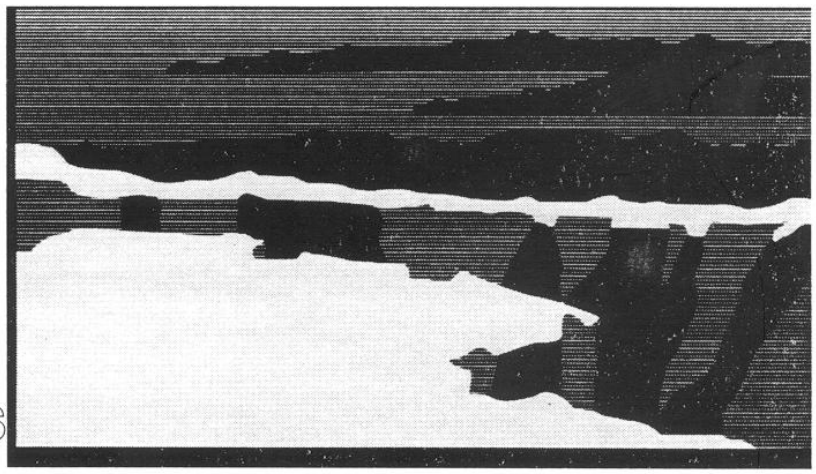

Los Alamos
NATIONAL LABORATORY

Form No. 836 R5
ST 2629 10/91

Los Alamos
NATIONAL LABORATORY

Tech-memo

LANSCE Division
Group LANSCE-1

To/MS: Dale Schrage, MS H817
From/MS: Richard LaFave, MS H817
Phone/FAX: 5-0029/5-2904
Symbol: LANSCE-1:01-002
Date: January 11, 2001
Email: rpl@lanl.gov

SUBJECT: Structural and RF Analysis of LANL 2 Gap, 350 MHz Spoke Resonator Cavity

Introduction:

As requested, a combined structural and RF analysis of the LANL 2-gap, 350 MHz spoke resonator has been performed. This memo summarizes the model predictions for maximum end flange deflections and reaction forces during tuning, cavity stress and deflections under vacuum loads, and resonant structural frequencies. In addition, predictions for shifts in resonant RF frequency are presented. The results shown in Tables 1 through 4 summarize the model predictions for the various conditions considered. Material properties are listed in Table 5.

Models:

Figures 1, 2a, and 2b show external and a section views of the cavity. Figures 3a and 3b show the section views along with some dimensions to indicate the overall size of the cavity. Although Figure 3a shows the annular stiffener diameter as 26 cm, 24 and 28 cm diameters were also considered. Four models of the spoke resonator have been constructed for MICAV and COSMOS/M. The first is a solid model of the RF volume that is used to predict RF resonant frequencies, while the three remaining models are shell models of the cavity structure with the various annular stiffener diameters mentioned previously. The structural models were constructed such that the resulting nodal displacements could be imposed directly on the RF volume model, resulting in resonant RF frequency shift predictions for the deformed geometries. Figures 4 and 5 show the mesh used in the RF volume model while Figures 6 and 7 show the structural mesh for the 26 cm diameter annular stiffener model. Material properties were taken as the ambient temperature niobium properties listed in Table 3 of LA-UR # 99-5826 and are reproduced in Table 4.

The RF model was meshed with four node tetrahedral elements resulting in problems with approximately 60,000 elements while the structural models were meshed with three node shell elements resulting in problems with approximately 10,000 elements.

Boundary Conditions:

Two sets of boundary conditions were imposed on each of the three structural models to simulate two methods of tuning the cavities. In the first the annular stiffeners are fully constrained while a fixed deflection is imposed on each of the bore tube end

flanges. In the second the fixed deflection is imposed on both the annular stiffeners and the bore tube end flanges. The amount of the fixed displacement was varied until the resulting peak stress reached the level specified in Table 1 of 7000 psi, corresponding to the yield point of room temperature niobium. Since the model was linear this trial and error procedure was trivial.

The cavities were also analyzed under vacuum loading conditions. In these cases both bore tube end flanges and both annular stiffeners were fully constrained while 2X atmospheric pressure (29.4 psi) was applied to all external surfaces.

Lastly the cavities were also analyzed in order to predict resonant structural frequencies. In these cases, as with the vacuum loading cases, both bore tube end flanges and both annular stiffeners were fully constrained.

Results and Discussion:

Results for each tuning sensitivity case considered are shown in Table 1. In an effort to test the MICAV RF predictions, similar simulations were run for the ANL 2-gap cavity for which some experimental results are available. Table 2 summarizes the MICAV predictions for the ANL cavity as well as some of the experimental results obtained by Tsuyoshi Tajima, Robert Gentzlinger, and Alan Shapiro. It should be noted that the MICAV RF predictions show good agreement with available data. This is a significant benefit since in the past MICAV has only been tested against other computer codes without the benefit of experimental data.

The maximum tuning sensitivity of 46 KHz/mil occurs with the 24 cm diameter annular stiffener although there is not a large difference in the sensitivity between the various sizes of stiffeners. As the table indicates, the significant improvement in tuning sensitivity occurs when driving the annular stiffener along with the bore tube end flange as opposed to fixing the stiffener. Figures 8 and 9 are typical of the stress and displacement plots for the case when the stiffener and end flange are driven together.

Table 3 lists the results for the vacuum loading cases and indicates peak stresses with 2X atmospheric pressure of 5181 psi, 74% of the room temperature yield strength of niobium. As the table indicates there is not a significant difference between the various sizes of stiffeners. Figures 10 and 11 are stress and displacement plots for the vacuum loaded 26 cm diameter cavity. These figures show that the areas of peak stress are in the spoke and not on the cavity exterior, so they are not affected significantly by the size of stiffener.

Table 4 summarizes the resonant structural frequency predictions and indicates a very stiff structure with the lowest structural resonant frequency predicted to be 270 Hz.

Summary:

A structural analysis of the 2-gap, 350 MHz spoke resonator cavity has been performed in order to determine maximum end flange deflections and flange reaction forces during tuning, cavity stress and deflections under vacuum loads, and resonant structural frequencies. The analysis indicates that there is not a significant variation in performance with stiffener diameter over the range considered, however a significant improvement in tuning sensitivity can be realized by moving the annular stiffeners with

the bore tube end flanges. This improvement stems from the larger endwall deflections that can be imposed on the structure in this configuration before peak stresses reach 7000 psi.

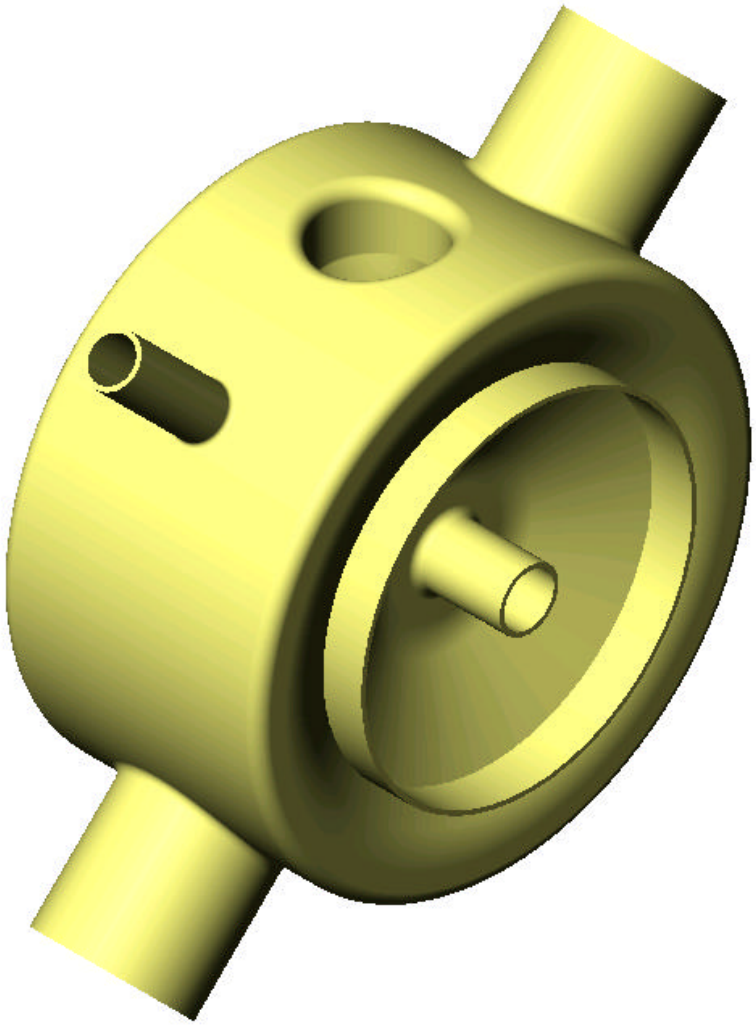

Figure 1: External View of LANL 2 Gap Cavity - Solidworks

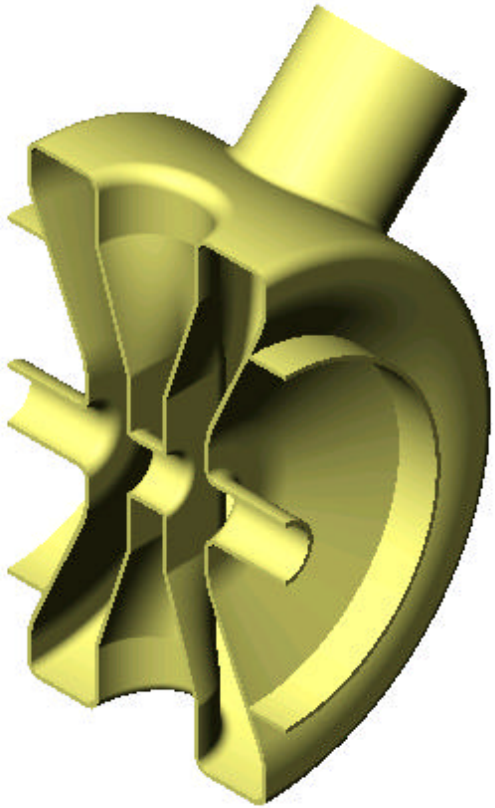

Figure 2a: Section View of LANL 2 Gap Cavity

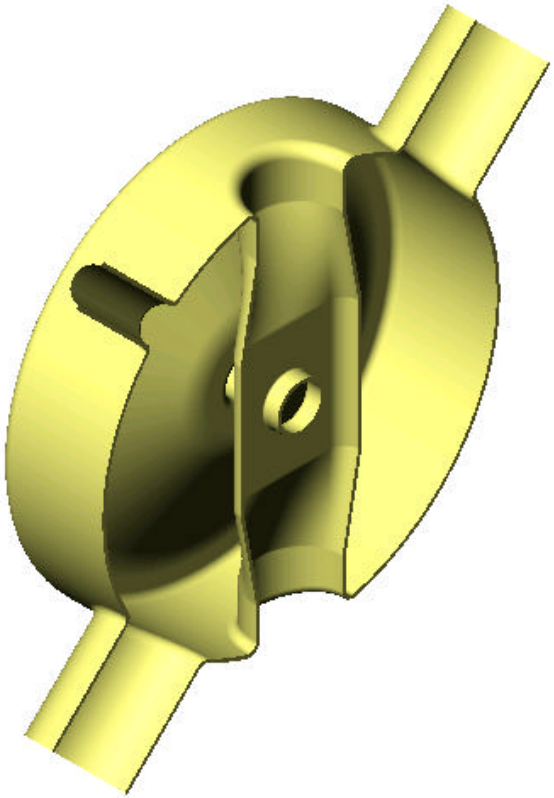

Figure 2b: Section View of LANL 2 Gap Cavity

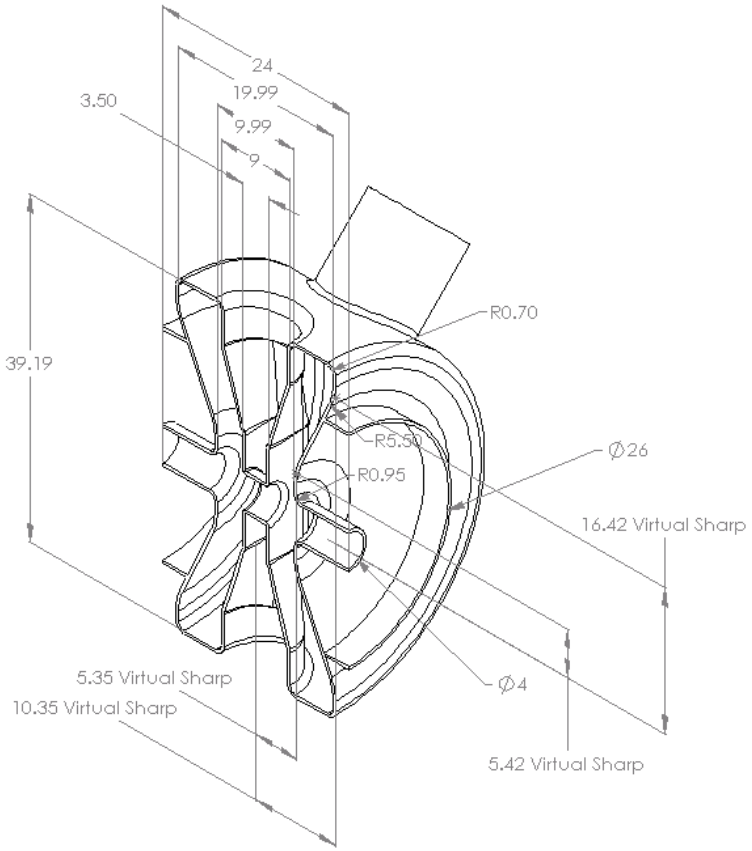

Figure 3a: Lateral Cavity Section View with Dimensions All Dims cm.

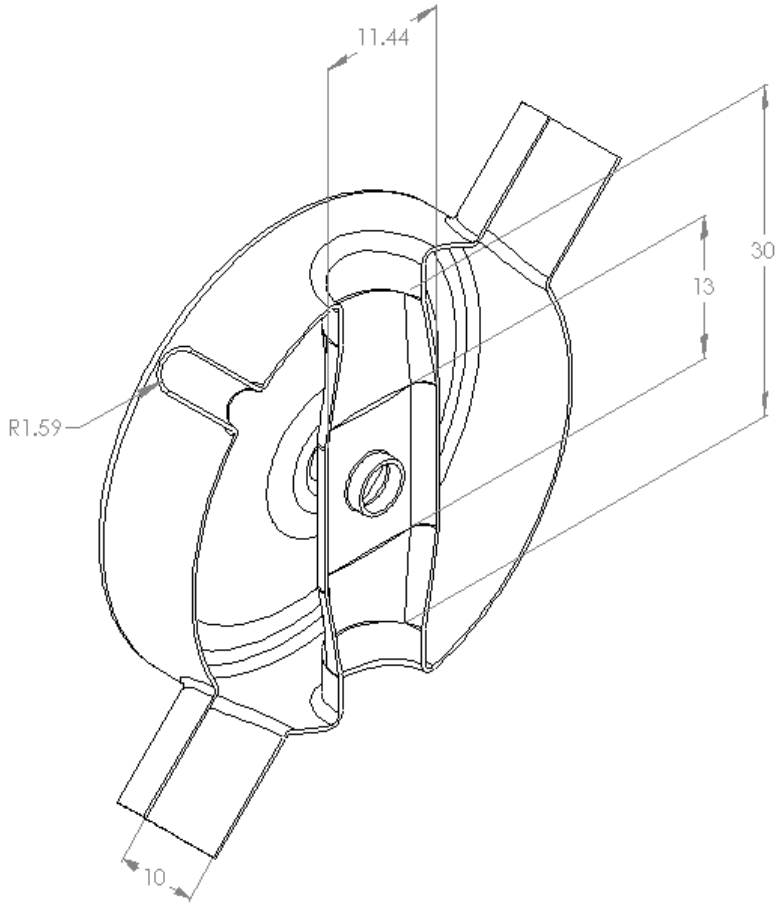

Figure 3b: Lengthwise Cavity Section View with Dimensions, All Dims cm.

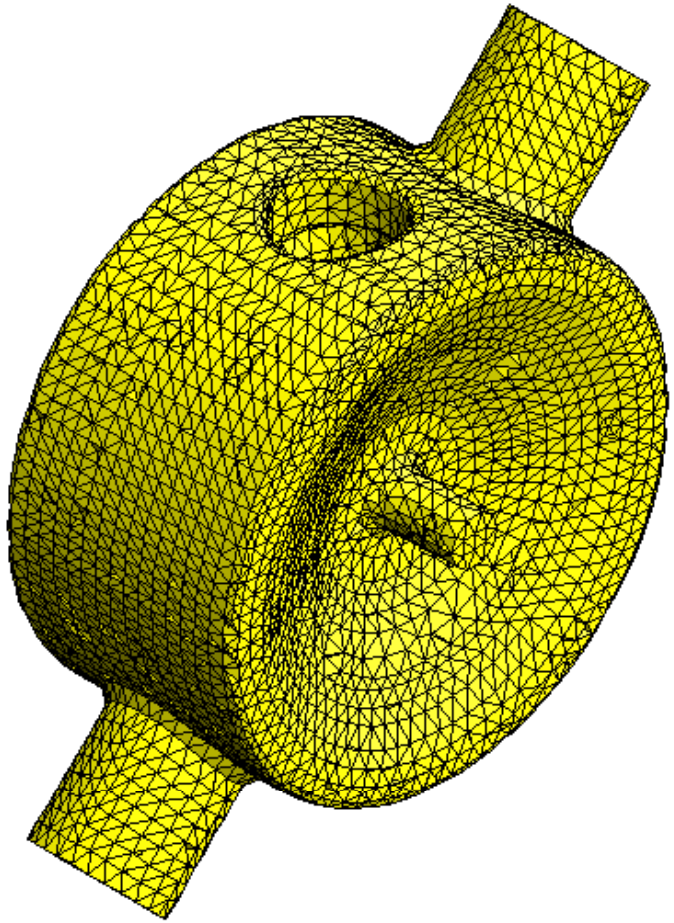

Figure 4: RF Volume Mesh

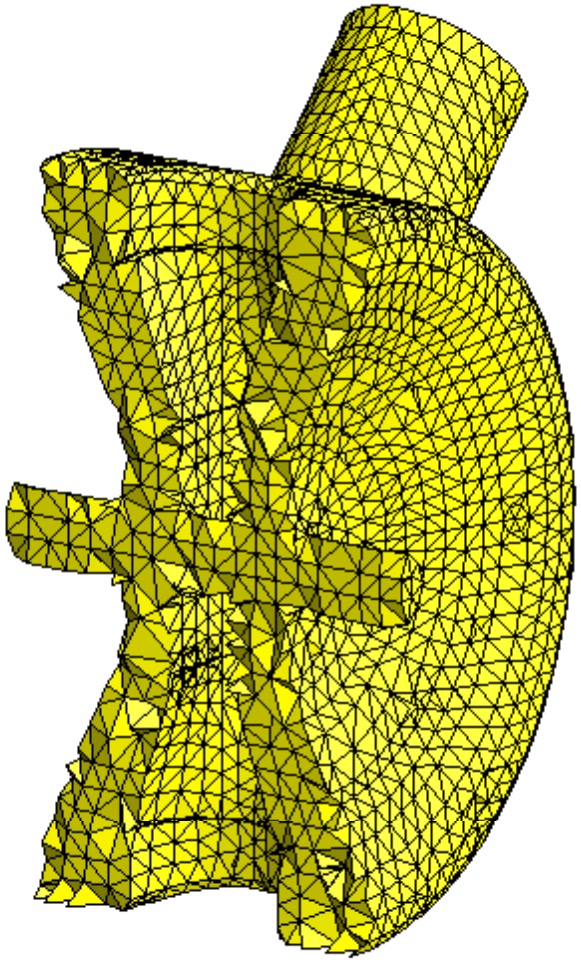

Figure 5: RF Volume Mesh, Cutaway View

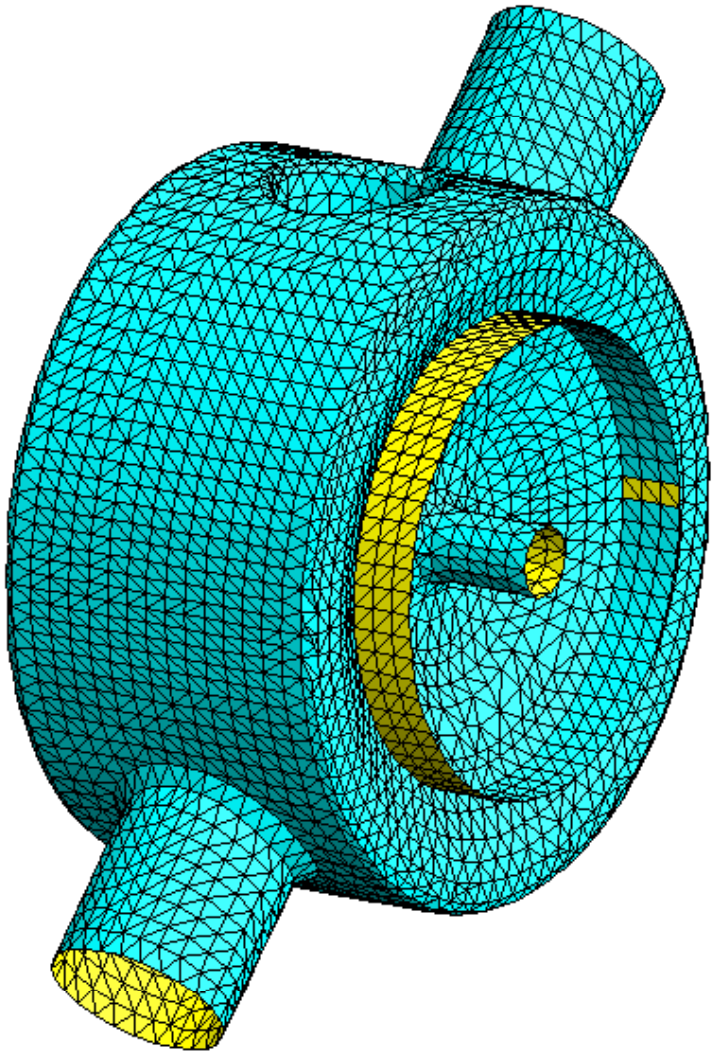

Figure 6: Structure Shell Mesh

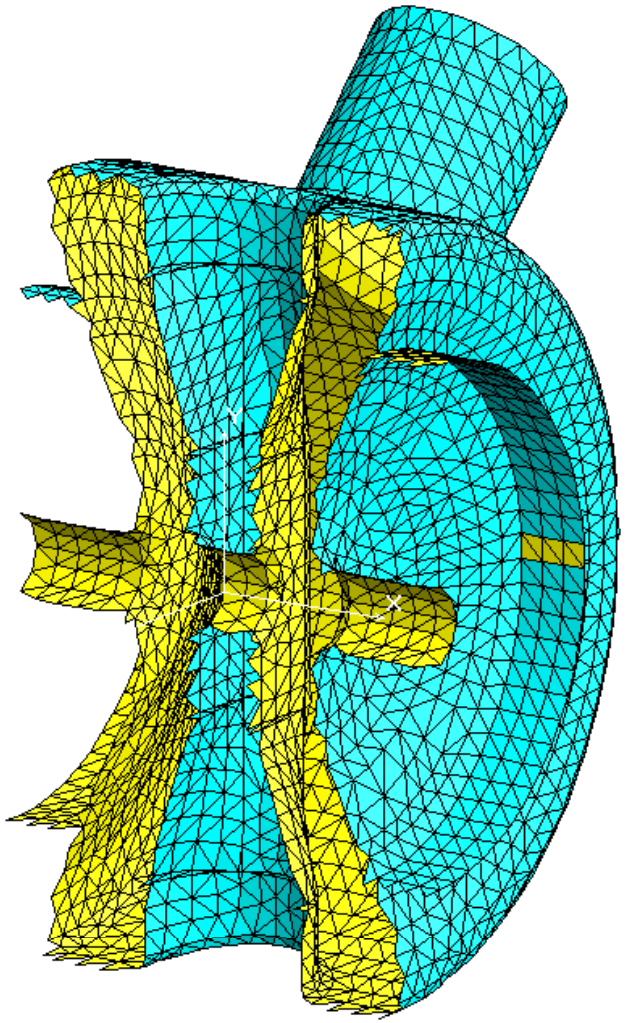

Figure 7: Structure Shell Mesh, Cutaway View

Figure 8: Von Mises Stress Plot, 26 cm Stiffener, Stiffener and Flange move together

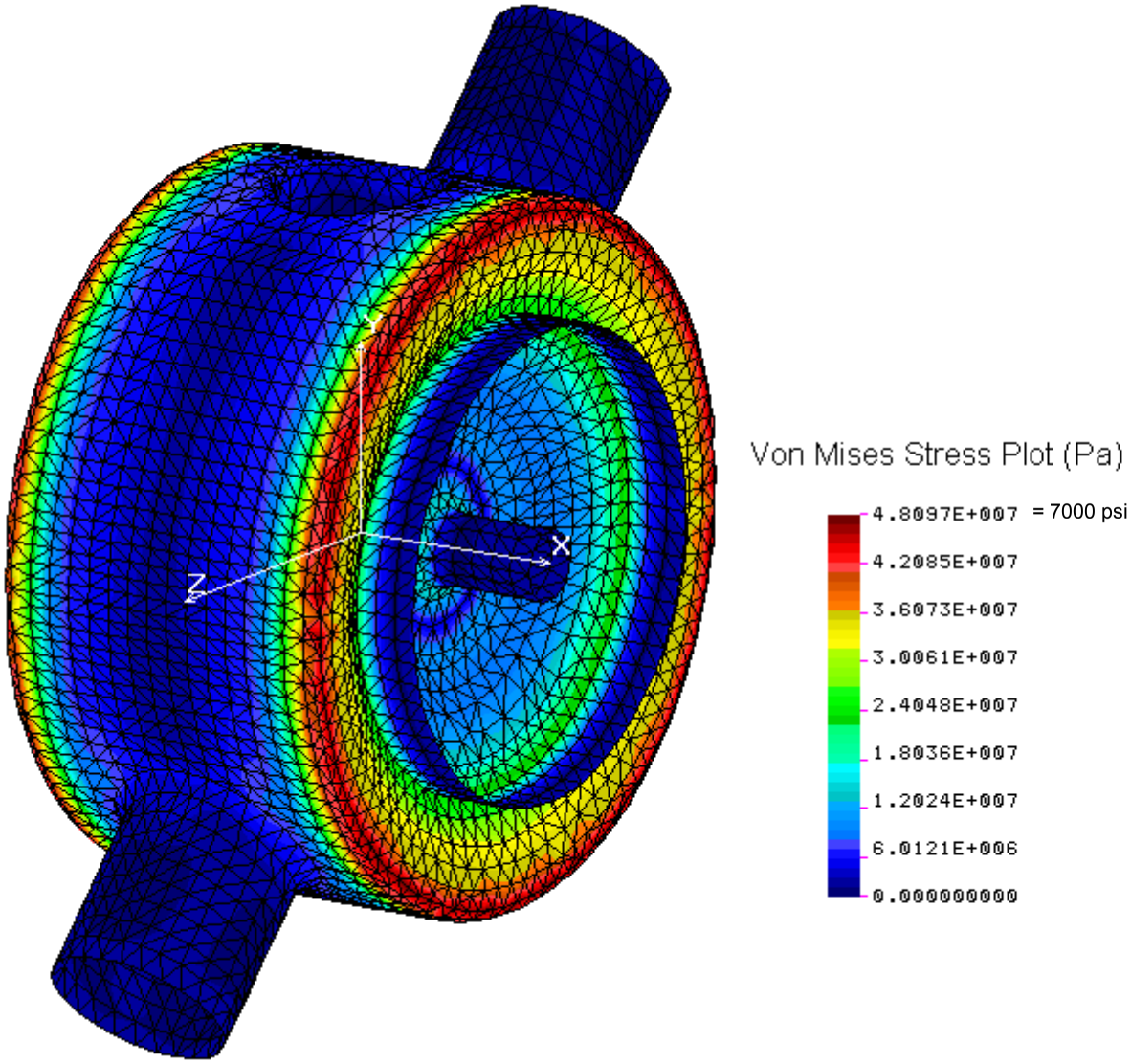

Figure 9: Displacement Plot, 26 cm Stiffener, Stiffener and Flange Move Together

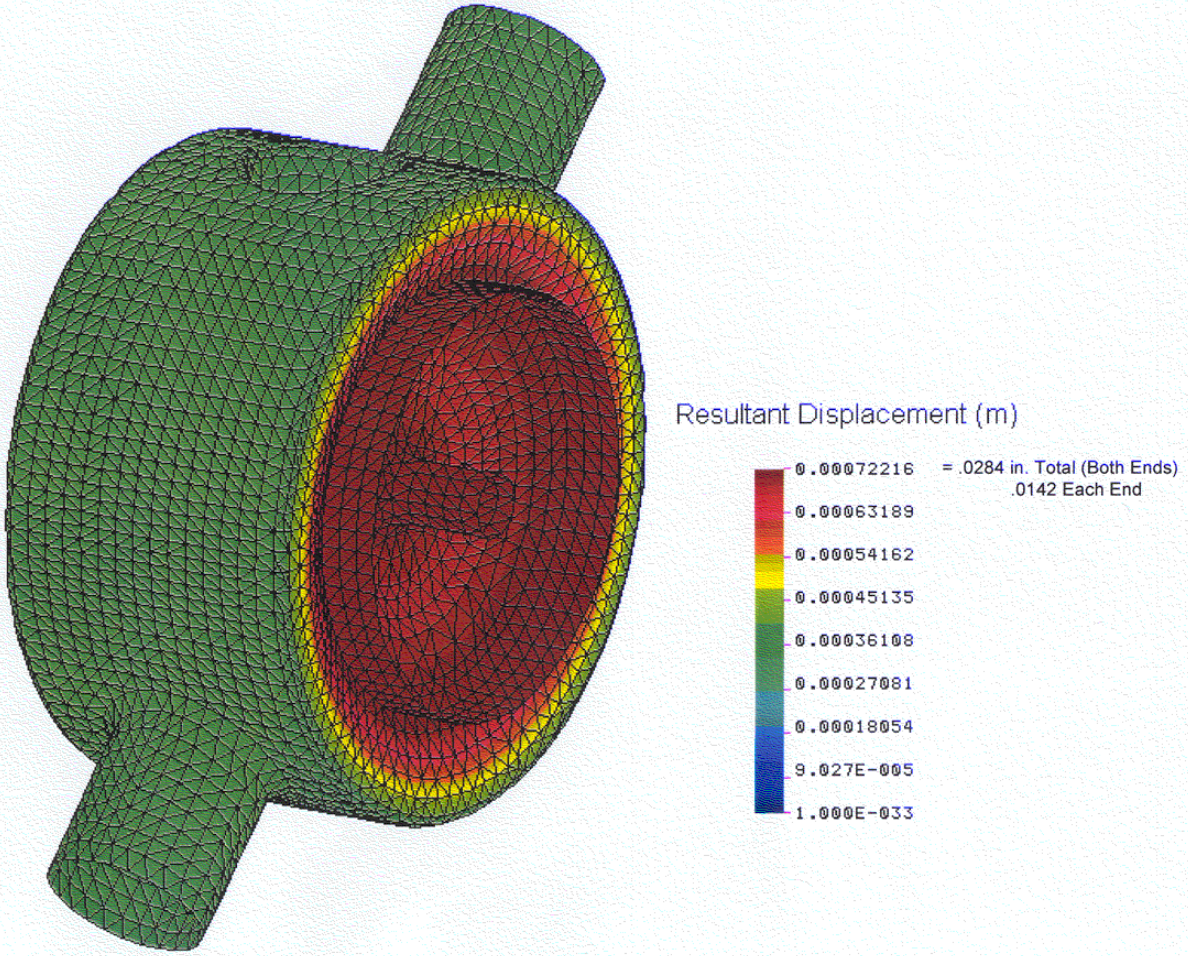

Figure 10: Von Mises Stress Plot, 26 cm Diameter Stiffener, 2X Vacuum Load, Cutaway View

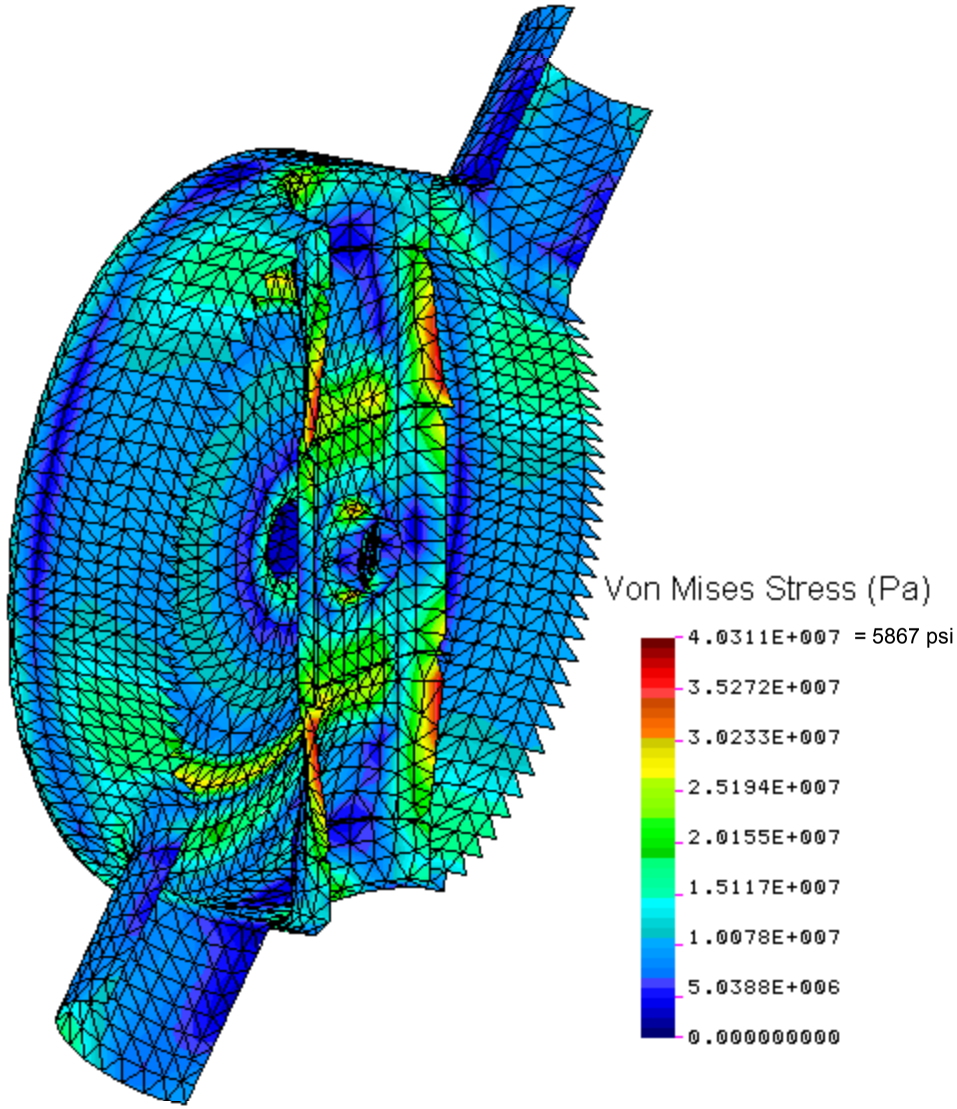

Figure 11: Displacement Plot, 26 cm Diameter Stiffener, 2X Vacuum Load, Cutaway View

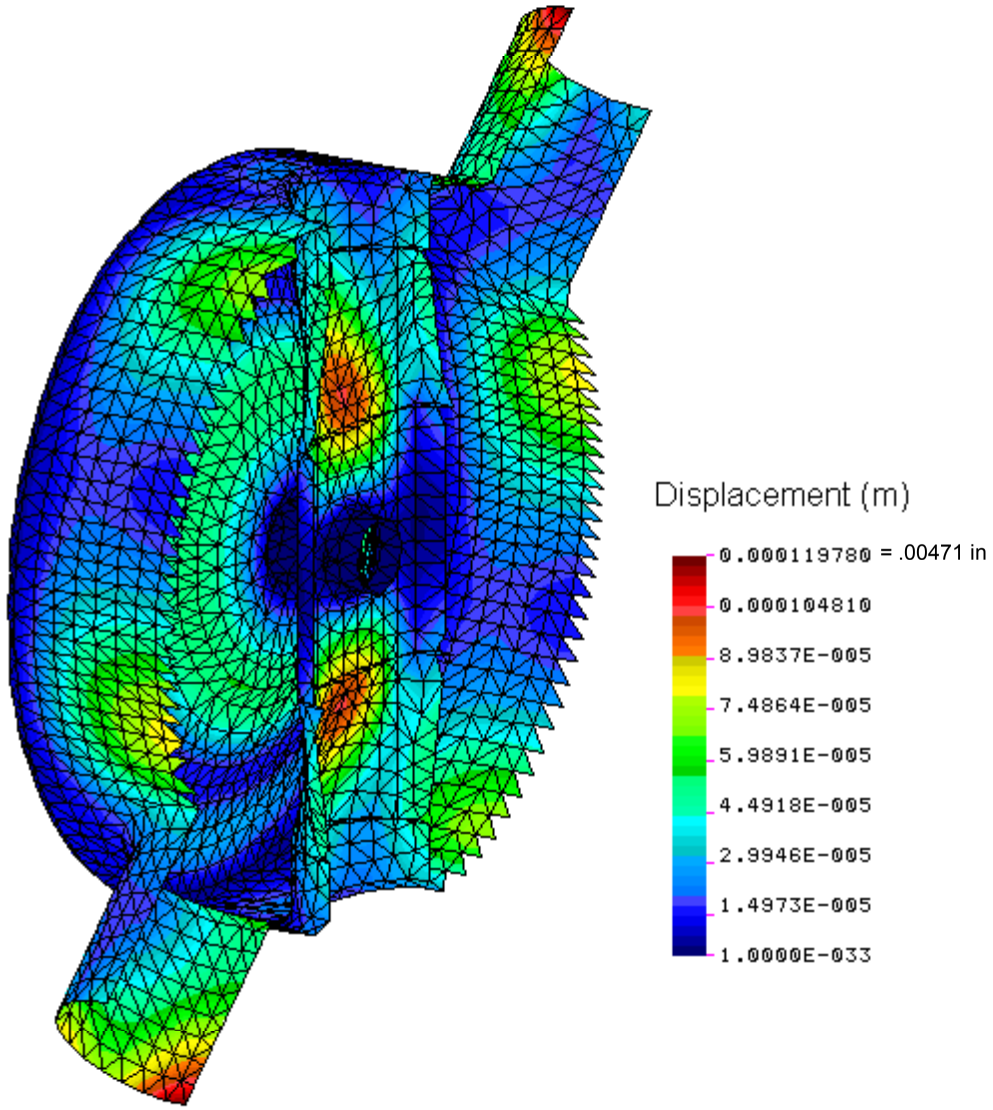

Annular Stiffener Dia. (cm)	Stiffener Boundary Condition	Total Reaction Force (lbs)	Peak Von Mises Stress (psi)	Displacement (Each End) (m)	Displacement (Each End) (in)	RF Resonant Frequency (MHz)	RF Frequency Shift (KHz)	Tuning Sensitivity (KHz/mil)	Tuning Sensitivity (KHz/lb)	Equiv Spring Stiffness (lb/mil)
28	Moves With Flange	1701	7000	0.000339	0.0133	350.714139	-602.565	-45.148	-0.3542	127.450
28	Fixed	457	7000	0.000140	0.0055	351.174658	-142.046	-25.845	-0.3108	83.151
26	Moves With Flange	1649	7000	0.000361	0.0142	350.671264	-645.440	-45.404	-0.3914	116.000
26	Fixed	402	7000	0.000139	0.0055	351.175857	-140.847	-25.664	-0.3504	73.248
24	Moves With Flange	1662	7000	0.000368	0.0145	350.649922	-666.782	-46.076	-0.4012	114.847
24	Fixed	399	7000	0.000139	0.0055	351.177459	-139.245	-25.370	-0.3490	72.697

Table 1: Stress and Deflection During Tuning
Unperturbed RF Resonant Frequency = 351.316704 MHz

	Measured	MICAV COSMOS/M	Error
Resonant Frequency (MHz)	339.699401	338.821495	0.26%
Tuning Sensitivity (MHz/in)	9.356	11.32	21.03%
Structural Stiffeness (lb/mil)	34.36	44.4	29.22%
(KHz/lb)	0.272	0.255	6.35%

Table 2: ANL 2 Gap Cavity Results

Annular Stiffener Dia. (cm)	Boundary Condition	Total Reaction Force (lbs)	Peak Von Mises Stress (psi)	Peak Displacement (m)	Peak Displacement (in)	RF Resonant Frequency (MHz)	RF Frequency Shift (KHz)
28	Vacuum Load x 2	3875	5172	0.0001203	0.0047	351.221720	-94.984
26	Vacuum Load x 2	3776	5177	0.0001198	0.0047	351.228742	-87.962
24	Vacuum Load x 2	3743	5181	0.0001195	0.0047	351.241765	-74.939

Table 3: Stress and Deflection Under 2X Vacuum Load

Annular Stiffener Dia. (cm)	End Flange / Stiffener Boundary Conditions	Resonant Structural Frequencies (Hz)				
		F1	F2	F3	F4	F5
28	Fixed / Fixed	283.5	469.4	518.6	549.4	552.0
26	Fixed / Fixed	271.1	467.5	516.4	547.5	548.2
24	Fixed / Fixed	269.6	465.2	513.7	545.4	547.3

Table 4: Resonant Structural Frequencies

Property	Value	Units
Density	0.31	lb/in^3
Young's Modulus	$1.42X10^7$	lb/in^2
Yield Strength (300K)	7000	lb/in^2
Poisson's Ratio	0.38	none
Electrical Resistivity (300 K)	$17X10^{-6}$	ohm-cm
Electrical Resistivity (4 K)	$4.72X10^{-15}$	ohm-cm

Table 5: Material Properties of Niobium

CC:
K. C. Chan, APT/TPO, MS H816
P. Colestock, LANSCE-9, MS H851
J. Delayen, JLAB
R. Garnett, LANSCE-1, MS H817
R. Gentzlinger, ESA-DE, MS H821
D. Gilpatrick, LANSCE-1, MS H817
W. B. Haynes, LANSCE-9, MS H851
A. Jason, LANSCE-1, MS H817
J. P. Kelley, LANSCE-1, MS H817
F. Krawczyk, LANSCE-1, MS H817
P. Leslie, LANSCE-1, MS H817
M. Lynch, LANSCE-5, MS H818
W. Lysenko, LANSCE-1, MS H817
M. Madrid, AR/TPO, MS H816
T. Myers, Advanced Energy Systems
J. Rathke, Advanced Energy Systems
B. Rusnak, LLNL
D. Rees, LANSCE-5, MS H818
E. Schmierer, ESA-DE, MS H821
J. D. Schneider, APT/TPO, MS H816
S. Schriber, LANSCE-1, MS H817
R. Sheffield, APT/TPO, MS H816
K. Shepard, ANL
H. V. Smith, APT/TPO, MS H816
T. Tajima, LANSCE-1, MS H817
R. Valdiviez, LANSCE-1, MS H817
T. Wangler, LANSCE-1, MS H817
R. Wood, LANSCE-1, MS H817
K. Zeroonians, SRAC
LANSCE-1 Reading File, MS H817